Nontopological origin of the planar Hall effect in the type-II Dirac semimetal $NiTe_2$

Qianqian Liu, Fucong Fei,* Bo Chen, Xiangyan Bo, Boyuan Wei, Shuai Zhang, Minhao Zhang, Faji Xie, Muhammad Naveed, Xiangang Wan, Fengqi Song,† and Baigeng Wang

National Laboratory of Solid State Microstructures, Collaborative Innovation Center of Advanced Microstructures, and College of Physics, Nanjing University, Nanjing 210093, China

(Received 7 January 2019; published 10 April 2019)

We measure the low-temperature magnetic transport in a recently discovered type-II Dirac semimetal $NiTe_2$ and successfully observe the planar Hall effect (PHE) which is often attributed to the chiral anomaly of topological electrons. The planar Hall signals oscillate with the in-plane angle with a π period and reach the extremum at 45° and 135°, which can be ideally described by the theoretical formulas. However, by analyzing the in-plane anisotropic magnetoresistance, we find no negative longitudinal magnetoresistance. In addition, the $\rho_{xx} - \rho_{yx}$ parametric plot exhibits a "shock-wave" pattern. All the evidence show that the presented PHE in $NiTe_2$ originates from the trivial orbital magnetoresistance rather than the topological-nontrivial chiral anomaly.

DOI: 10.1103/PhysRevB.99.155119

I. INTRODUCTION

Topological semimetals (TSMs) are currently creating a surge of research activities in condensed matter physics due to their interesting properties. Multiple series of TSMs have been theoretically predicted and experimentally verified, such as Dirac semimetals, Weyl semimetals, and nodal-line semimetals, etc. Most of the TSMs, such as Cd_3As_2, Na_3Bi, TaAs [1–10], hold linear cone-shaped band dispersions. Point-like Fermi surface appears when the Fermi level aligns with the Dirac/Weyl points. Meanwhile, in some special TSMs, such as WTe_2, LaAlGe, VAl_3, and the $PtSe_2$ family [11–19], the Lorentz invariance is broken and the Dirac/Weyl cones are tilted strongly along a certain momentum direction. A pair of electron and hole Fermi pockets contact each other at the Dirac/Weyl point because of the tilting. This unique Fermi surface configuration is distinct from the traditional cases and these materials with Lorentz invariance breaking are called type-II TSMs. Accordingly, the previous mentioned TSMs with a point-like Fermi surface are named type-I TSMs. Special Fermi surface configurations in type-II TSMs are expected to result in many phenomena such as Klein tunneling in momentum space [20], anisotropic electrical transport [21], angle-dependent chiral anomaly [22], etc. Among these peculiar characteristics, the chiral anomaly has been concerned, and has been widely investigated in many TSMs. In Weyl semimetals, chiral charges pump between a pair of Weyl points under parallel electric and magnetic fields, resulting in a chiral current. When increasing the magnetic field, the negative magnetoresistance (NMR) can be experimentally observed [23–25]. The same scenario appears in Dirac semimetals as a Dirac point splits into two Weyl points with opposite chirality when applying magnetic field [25]. However, the NMR phenomenon cannot be used as a solid evidence to judge the existence of the chiral anomaly because other unexpected effects, such as extrinsic current jetting effects, may cause a similar phenomenon [26,27]. Recently, theories suggest that the planar Hall effect (PHE) is another transport evidence for the chiral anomaly in topological semimetals, where PHE refers to the transverse voltage when the magnetic and electric fields are coplanar [diagrammatically displayed in Fig. 3(b)] [28,29]. So far, PHE has been observed in both type-I and type-II TSMs such as $ZrTe_5$, Cd_3As_2, GdPtBi, VAl_3, $MoTe_2$, etc. [30–35]. It seems to be a general phenomenon that can be detected in many different kinds of TSMs. However, the origin of PHE is still not clear and cannot be briefly pinned down to the chiral anomaly in these materials. Several other effects such as magnetic order, spin-orbital coupling, and in-plane orbital magnetoresistance (MR) may also induce a similar phenomenon that needs to be carefully distinguished.

Here we report the observation of PHE and anisotropic magnetoresistance (AMR) in $NiTe_2$, which is a recently discovered type-II Dirac semimetal [36]. The Dirac points of $NiTe_2$ are close to the Fermi surface ($\sim$0.1 eV above the Fermi level, see the Supplemental Material, Fig. S1 [37]) and PHE induced by chiral anomaly is expected to be detected in this material. After the systematic study of the angle dependence of PHE and (MR under various temperatures, however, we conclude that the PHE in $NiTe_2$ originates from the trivial in-plane orbital MR rather than the expected chiral anomaly. Our result can be taken as an example that PHE measured in topological materials may not be caused by chiral anomaly. When PHE is detected in topological semimetals, one need to be more cautious to attribute it to the chiral anomaly or nontrivial Berry phase, and further detailed investigations are necessary.

II. RESULTS AND DISCUSSION

A. Crystal growth and characterization

The single crystals of $NiTe_2$ were grown by the self-flux method. Nickel powder (from Aladdin, 99.9%) and tellurium

*feifucong@nju.edu.cn
†songfengqi@nju.edu.cn

 ©2019 American Physical Society

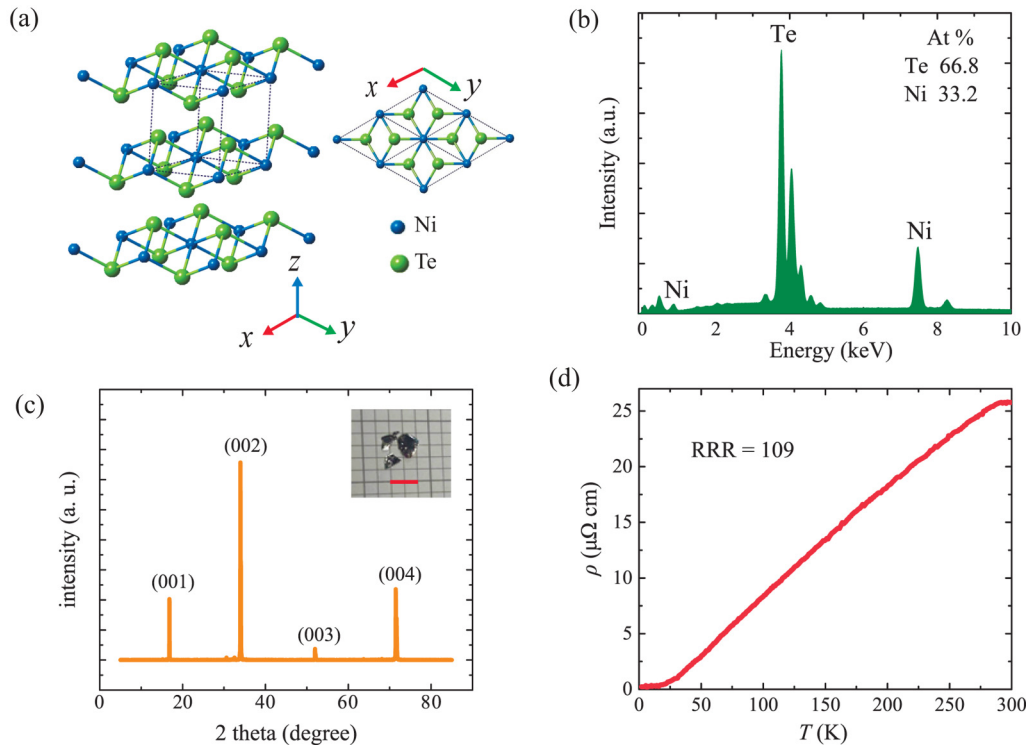

FIG. 1. The crystal growth and characterization of the $NiTe_2$ single crystals. (a) The CdI_2-type crystal structure of $NiTe_2$. (b) The EDS spectrum of synthesized $NiTe_2$ crystal, which demonstrates a stoichiometric ratio. (c) The single crystal x-ray-diffraction data of the (00n) surfaces of the sample. The inset is the optical micrograph of the $NiTe_2$ crystal, the scale-bar is 4 mm. (d) The resistivity varies with temperature at zero field.

shot (from Alfa Aesar, 99.99%) were mixed with a molar ratio of 1:15 in a glove box and sealed in an evacuated quartz tube. The quartz tube was then heated to 700 °C quickly in a muffle furnace and kept at this temperature for 12 h, before being slowly cooled down to 500 °C (3 °C/h), The excess amount of Te was centrifuged at 500 °C. Millimeter-size crystals with the shiny surface can be obtained. $NiTe_2$ crystal holds a CdI_2-type trigonal structure with the $P\bar{3}m1$ space group. It is a layered material and the single layers of $NiTe_2$ stack along the c axis, as shown in Fig. 1(a). Figure 1(b) describes the energy dispersive spectrum (EDS) of one typical crystal. One can clearly see the Ni and Te peaks with a perfect atomic ratio of 1:2. Clear (00n) diffraction peaks of the $NiTe_2$ can be seen in the single crystal x-ray diffraction pattern in Fig. 1(c), and there are no other impurity peaks, indicating the high quality of the crystals. In Fig. 1(d), the resistance versus temperature exhibits a metal behavior, and the residual resistance ratio is 109 at zero field. Figure 2(a) indicates the magnetoresistance under various temperatures when the magnetic field is perpendicular to the sample surface. We noticed that the MR ratio ($(\rho(B)-\rho(0))/\rho(0)$) of the sample is relatively larger, reaching as high as 281% at 2 K and 8 T. Besides, the MR at low temperature is quite linear, which is consistent with previously reported [36]. In Fig. 2(b), the MR ratio under different temperatures is reduced by 14 times from 2 to 50 K when the magnetic field is 8 T. Figure 2(c) shows the longitudinal resistivity varies with different angles when magnetic field is rotating out of the x-y plane as shown in the inset schematic diagram, and the out-of-plane AMR can be obviously seen. Figure 2(d) shows the Hall resistivity of the sample. The bended Hall curves indicate the multiband electrical transport channels in $NiTe_2$, which is consistent with the band structure calculations of this material [36].

B. Measurement of planer Hall effect

In the next step, we rotated the direction of magnetic field into the x-y plane (a-b plane of the $NiTe_2$ crystal) and measured the in-plane PHE and AMR. Quantitatively, the resistivity tensor considering chiral anomaly can be written as [28]

$$\rho_{yx}^{\mathrm{PHE}} = -\Delta\rho^{\mathrm{chiral}}\sin\theta\cos\theta, \tag{1}$$

$$\rho_{xx} = \rho_{\perp} - \Delta\rho^{\mathrm{chiral}}\cos^2\theta, \tag{2}$$

where ρ_{yx}^{PHE} represents the in-plane hall resistivity that directly shows the PHE. The $\Delta\rho^{\mathrm{chiral}}=\rho_{\perp}-\rho_{\parallel}$ is the chiral anomaly induced resistivity anisotropy, $\rho_{\perp}$ and $\rho_{\parallel}$ represent the resistivity with the magnetic field perpendicular (90°) and parallel (0°) to the electric current respectively. ρ_{xx} is the AMR when magnetic field rotating in the sample plane as shown in the inset of Fig. 3(b). Both ρ_{yx}^{PHE} and ρ_{xx} hold a period of 180°. In particular, for ρ_{yx}^{PHE}, the valleys appear at 45° and 225° whereas the peaks appear at 135° and 315°, which is distinct from the angular dependence measured in an ordinary Hall effect when magnetic field is perpendicular to the sample x-y plane, which holds a period of 360°. The device configuration is illustrated in the inset of Fig. 3(b), with two longitudinal electrodes measuring the in-plane longitudinal MR and other two lateral electrodes measuring the PHE signal. The applied magnetic field rotates within the sample surface and θ

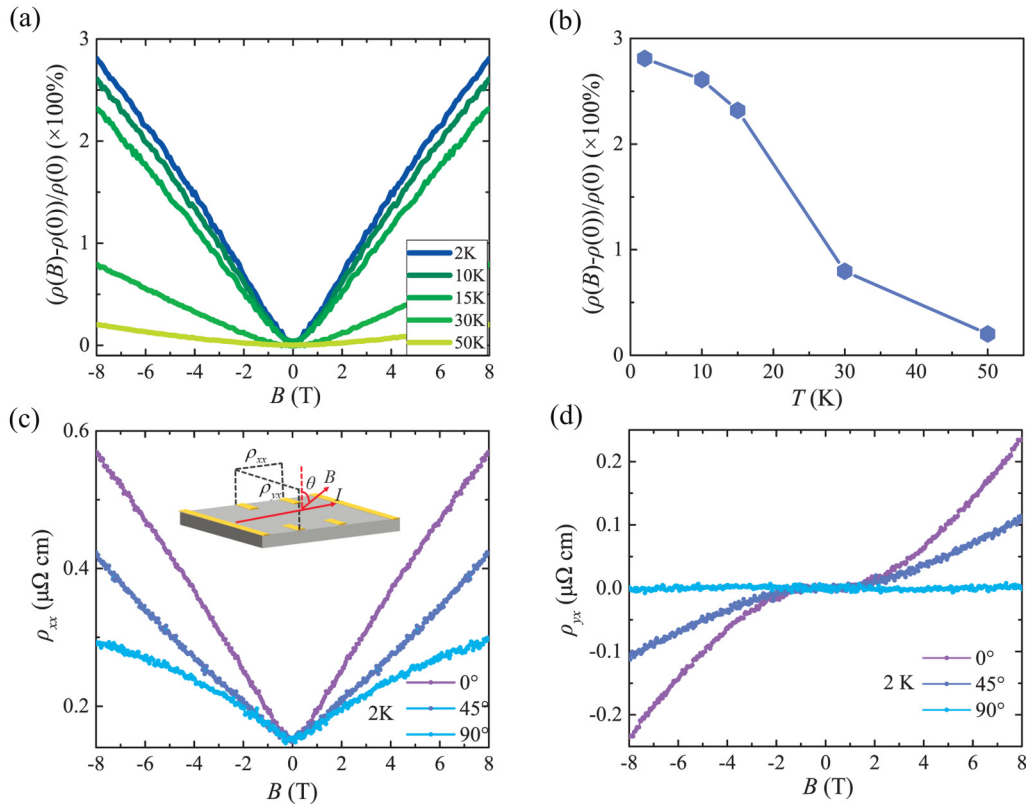

FIG. 2. The transport properties of the $NiTe_2$ single crystals. (a) The MR at different temperatures when the magnetic field is perpendicular to the x-y plane. (b) The MR ratio varies with different temperatures ($B = 8$ T). (c) The longitudinal resistivity varies with different angles when the magnetic field is rotating out of the x-y plane ($T = 2$ K). The inset displays the device configuration for out-of-plane transport measurement. (d) The Hall resistivity measured at different angles when magnetic field is rotating out of the x-y plane ($T = 2$ K).

represents the angle between the in-plane magnetic field and the applied electric current. It is worth mentioning that in practical cases, there are several misalignments that may influence the PHE measurement. First, the magnetic field commonly does not rotate in the plane strictly and a residual out-of-plane component may exist, which will generate a normal Hall signal mixing into the real in-plane response and affect the measurement of PHE. To separate the normal Hall contribution, we measured the transport signal under both positive and negative field and calculated the average of the positive/negative data, as the normal Hall signal is opposite when reversing the field direction while the PHE signal holds the same. Second, if two Hall electrodes are deviated from each other longitudinally, in-plane longitudinal AMR and out-of-plane longitudinal MR signals will be induced. The former one possesses a $\cos^2\theta$ angle relation that can be ruled out if processing the data by the formula $\rho_{yx} = (\rho_{yx}(\theta) - \rho_{yx}(\pi - \theta))/2$. The latter out-of-plane longitudinal MR contribution is troublesome as it is $\cos^2(\theta + \delta)$ dependence and the phase shifting δ is stochastic depending on the geometrical relationship between the current and magnetic field direction. We measured several samples and find that the PHE data always show the peak near 135° (315°) and the valley near 45° (225°). Therefore we believe that this out-of-plane MR with random phase is small and can be ignored. After considering all these items, we plotted the intrinsic PHE signal in Fig. 3(a) and one can see that experimental data demonstrate a period of 180° period, with valleys at 45° and peaks at 135°, which fit well with the fitting curves (red lines) based on Eq. (1). We plotted the planar Hall coefficient $\Delta\rho_{yx}$ versus magnetic field in Fig. 3(b). The solid line is the power law fitting curve of the data points, showing the field dependence with an exponent of 1.41. According to the previous theoretical calculation, if the PHE signal purely originates from chiral anomaly, $\Delta\rho_{yx}$ should be proportional to B^2 [29]. The deviation of the exponent indicates that the PHE may not originate from pure chiral anomaly. To demonstrate the behavior of PHE in more detail, we research the temperature-dependent amplitude of the PHE at 14 T. The amplitude persists until 150 K as shown in Fig. 3(c) and the planar Hall coefficients $\Delta\rho_{yx}$ at different temperatures are extracted from fitting data in Fig. 3(d) by Eq. (1). It is clear that $\Delta\rho_{yx}$ decreases quickly from 2 to 60 K, and the rate of decline gradually slows down at higher temperatures. It is reduced by almost five times at 150 K compared with the PHE signal at 2 K.

C. Origin of measured planer Hall effect

From the PHE measurement and the analysis that is mentioned above, though it fits well with Eq. (1), it is still hard to figure out whether the measured PHE signal truly comes from chiral anomaly or it is just a trivial phenomenon caused by some other factors. Therefore, we next focus on the in-plane longitudinal AMR signals measured simultaneously. Figure 4(a) indicates the measured in-plane AMR under different fields at 2 K. As the field rotates, a pronounced

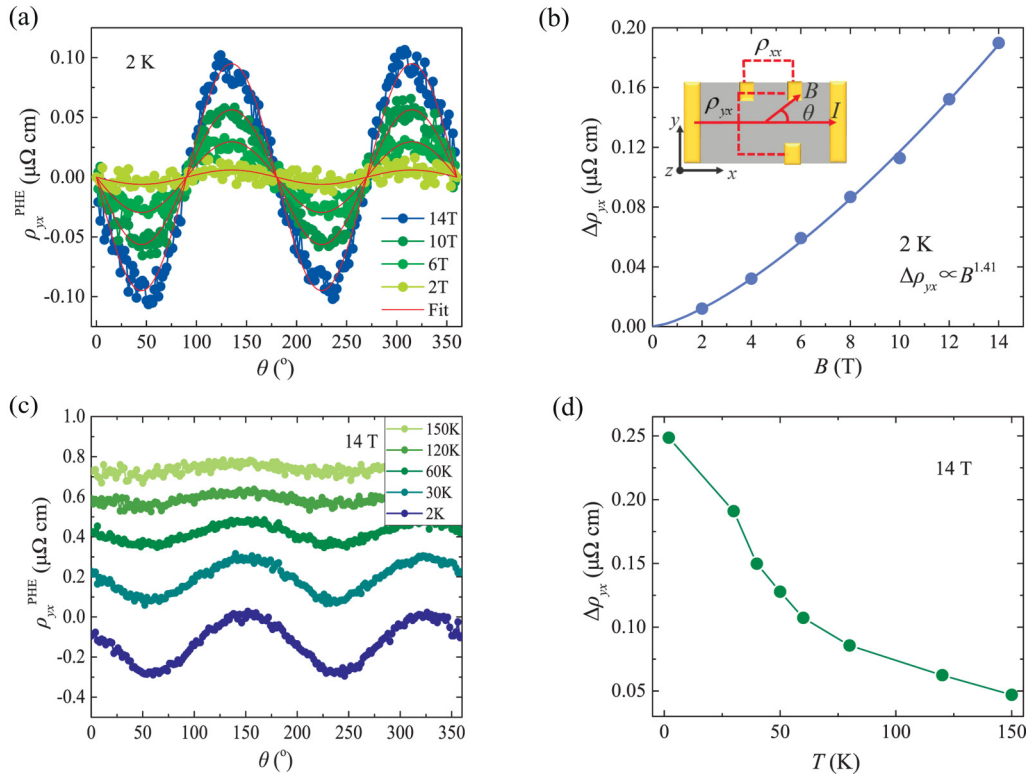

FIG. 3. Planar Hall effect measurement in $NiTe_2$. (a) The measured PHE data and the corresponding fitting curves under different B fields ($T = 2$ K). (b) The amplitude of PHE varies with magnetic field ($T = 2$ K). The inset shows the schematic of the device configuration for PHE measurement. (c) Angle dependence of the planar Hall resistivity taken at different temperatures ($B = 14$ T). (d) The amplitude of PHE varies with temperature ($B = 14$ T).

modulation of longitudinal resistivity is observed, with a period of 180°. Using Eq. (2) to fit the experimental data, one can find that the fitting curves (red lines) have a good agreement with the experiment. The $\Delta\rho_{xx}$ at different fields which can be further fitted to the power law curve with $\Delta\rho_{xx} \propto B^{1.41}$, as shown in Fig. 4(b), the fitting exponent is consistent with the result in Fig. 3(b), confirming the reliability and analyses of our measurements. The PHE and AMR curves show the $\sin\theta\cos\theta$ and $\cos^2\theta$ dependence, respectively, and both are consistent with the equations described by pure chiral anomaly. However, one can find that in Fig. 4(a), when magnetic field is parallel to the electrical current (0° and 180°), the longitudinal resistivity increases when increasing the magnetic field and exhibits a positive MR. This result is clearly in contrast to the NMR caused by chiral anomaly. As mentioned above, Eqs. (1) and (2) are ideal equations that only take the chiral anomaly into consideration. Namely, for ρ_{xx}, NMR should be displayed. In addition, in the pure chiral anomaly case, the resistivity ($\rho_\perp$) should keep constant when the magnetic field is perpendicular to the current and the resistivity ($\rho_\parallel$) should decrease as B increases when the magnetic field is parallel to the current [30,33]. In Fig. 4(c), we plotted the extracted $\rho_\perp$ and $\rho_\parallel$ from Fig. 4(a) with the variation of magnetic fields. It can be seen that $\rho_\perp$ changes linearly with B and $\rho_\parallel$ changes relatively slowly, which satisfies the relation of the polynomial. Both $\rho_\perp$ and $\rho_\parallel$ increase when increasing the magnetic field, which is distinct from the case of the chiral anomaly. As a result, we consider that the chiral anomaly is not the origin of our measured PHE result.

To unveil the real factors leading to this kind of PHE signal, we temporarily set aside the specific system with chiral anomaly and take a general electric conductor system into consideration. If the in-plane magnetic field causes the in-plane anisotropic resistivity in this system and then the resistivity tensor can be written as

$$\begin{pmatrix} E_{x'} \\ E_{y'} \end{pmatrix} = \begin{pmatrix} \rho_\parallel & 0 \\ 0 & \rho_\perp \end{pmatrix} \begin{pmatrix} j_{x'} \\ j_{y'} \end{pmatrix}, \tag{3}$$

where the direction x' is the direction of B to be applied and the direction y' is perpendicular to the field. If we take the sample itself as the coordinate system, after executing a standard coordinate transformation procedure, Eq. (3) becomes:

$$\begin{aligned} \begin{pmatrix} E_x \\ E_y \end{pmatrix} &= \begin{pmatrix} \cos\theta & -\sin\theta \\ \sin\theta & \cos\theta \end{pmatrix} \begin{pmatrix} \rho_\parallel & 0 \\ 0 & \rho_\perp \end{pmatrix} \begin{pmatrix} \cos\theta & \sin\theta \\ -\sin\theta & \cos\theta \end{pmatrix} \begin{pmatrix} j_x \\ j_y \end{pmatrix} \\ &= \begin{pmatrix} \rho_\parallel\cos^2\theta + \rho_\perp\sin^2\theta & (\rho_\parallel - \rho_\perp)\sin\theta\cos\theta \\ (\rho_\parallel - \rho_\perp)\sin\theta\cos\theta & \rho_\parallel\sin^2\theta + \rho_\perp\cos^2\theta \end{pmatrix} \begin{pmatrix} j_x \\ j_y \end{pmatrix}. \end{aligned} \tag{4}$$

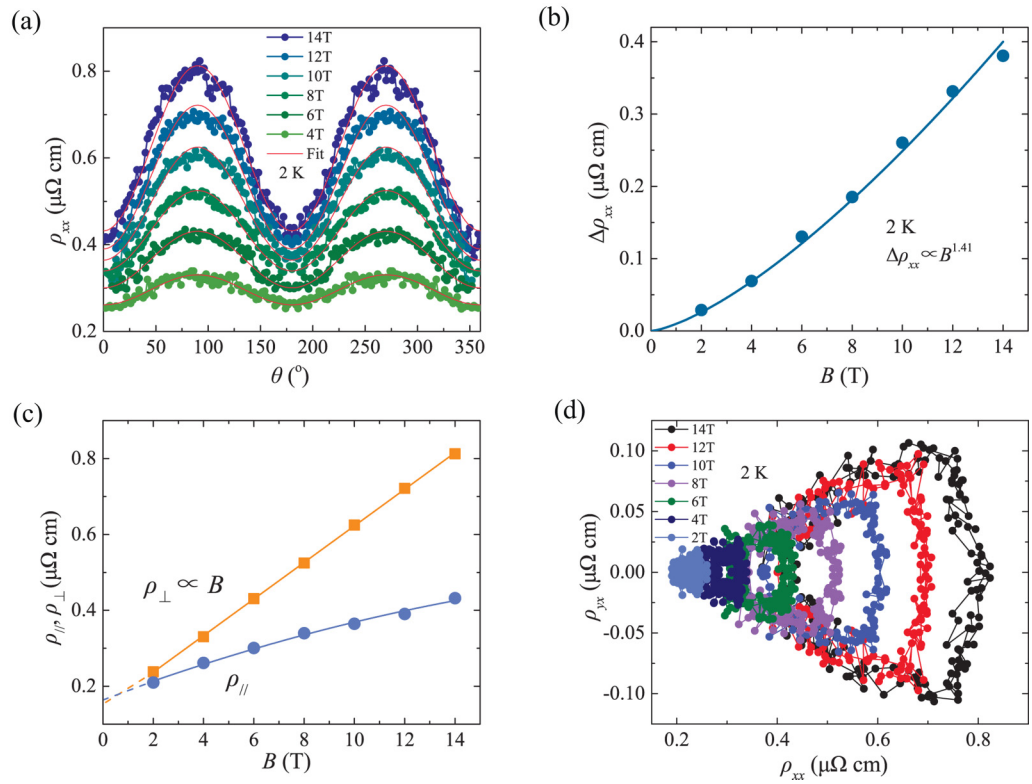

FIG. 4. Nontopological origin of the PHE in $NiTe_2$. (a) Measured in-plane AMR versus angle θ at various fields ($T = 2$ K). Solid red curves represent the best fitting curves by using Eq. (2). (b) The amplitude of AMR varies with magnetic field at 2 K. The solid curve is the power law fit curve for the experimental data points. (c) $\rho_{\perp}$ and $\rho_{\parallel}$ extracted from the experimental data in panel (a). The orange and blue solid curves represent the power law fit curves for $\rho_{\perp}$ and $\rho_{\parallel}$, respectively. (d) The orbits obtained by plotting ρ_{xx} and ρ_{yx} with angle θ as the parameter at specific magnetic fields. The orbits evolve to form a "shock-wave" pattern, indicating the absence of chiral anomaly.

If the direction x is parallel to the electric current, i.e. $j_y = 0$ and θ is the angle between applied electric and magnetic fields, then we get

$$\rho_{yx} = E_y/j_x = -(\rho_{\perp} - \rho_{\parallel}) \sin\theta \cos\theta, \quad (5)$$

$$\rho_{xx} = E_x/j_x = \rho_{\perp} - (\rho_{\perp} - \rho_{\parallel})\cos^2\theta. \quad (6)$$

One may find that the form of Eqs. (5) and (6) is exactly the same as Eqs. (1) and (2). That is to say, the PHE can be observed as long as the resistivity is anisotropic when applying an in-plane magnetic field. The AMR may be caused by various reasons, not only chiral anomaly, but also classical orbital MR, strong spin-orbital coupling in magnetic systems, etc. The similar derivation process was also reported previously [38], and the PHE has been experimentally reported not only in TSMs but also in topological insulators [39,40], magnetic material (Ga,Mn)As devices [41], trivial metal Bismuth [38], and so on. $NiTe_2$ is a nonmagnetic bulk three-dimensional material with complicated Fermi surface configurations (see the Supplemental Material, Fig. S2 [37]). The anisotropic orbital MR is pretty common in this kind of system and the out-of-plane AMR is also clearly demonstrated by our experiment [Fig. 2(c)]. It is well known that the transport property of a material is closely related to the specific configuration of the Fermi surface. If there are multiple Fermi pockets or the morphology of the Fermi pockets are complicated, when carriers are moving towards different directions, transport parameters such as mean scattering time, effective mass, and mobility, etc., vary greatly. This kind of difference is also reflected in the magnetoresistance along different directions, leading to an anisotropic orbital MR. Therefore, there are reasons to attribute PHE in $NiTe_2$ to its in-plane anisotropic orbital MR. For further evidence, referring to a recent report giving a plausible criterion for the chiral anomaly [38], we plotted the amplitude of PHE vs in-plane AMR of $NiTe_2$ with θ as a parameter under a specific magnetic field in Fig. 4(d). The parametric plot pattern of the system in which the PHE is dominated by chiral anomaly, such as Na_3Bi and GdPtBi, are concentric around the center [38]. In contrast, in our measurement of $NiTe_2$, as the B field increases, the orbits evolve to form a "shock-wave" pattern, which is a typical exemplification with the absence of chiral anomaly. Therefore, our opinion that the PHE of $NiTe_2$ is not from chiral anomaly or nontrivial Berry curvature is further confirmed.

III. CONCLUSION

We measured the PHE in the type-II Dirac semimetal $NiTe_2$. By carefully analyzing the data received, we found that the PHE in $NiTe_2$ does not originate from expected chiral anomaly and the PHE signal can be detected as long as the

resistivity of a solid system is anisotropic when applying an in-plane magnetic field. We believe that the PHE we measured in $NiTe_2$ stems from its in-plane orbital MR. Our result can be taken as an example that PHE measured in topological materials is caused by a nontopological origin. In addition, it is necessary to point out that PHE measured in topological materials cannot originate from a chiral anomaly or nontrivial Berry phase when NMR is absent. In such studies, special attention is needed and one should take both PHE and NMR into consideration to distinguish the real origin of the PHE signals.

ACKNOWLEDGMENTS

The authors gratefully acknowledge the financial support of the National Key R&D Program of China (2017YFA0303203), the National Natural Science Foundation of China (91622115, 11522432, 11574217, U1732273 and U1732159), the Natural Science Foundation of Jiangsu Province (BK20160659), the Fundamental Research Funds for the Central Universities, and the opening Project of the Wuhan National High Magnetic Field Center.

Q.L. and F.F contributed equally to this work.

[1] S. M. Huang, S. Y. Xu, I. Belopolski, C. C. Lee, G. Q. Chang, B. K. Wang, N. Alidoust, G. Bian, M. Neupane, C. L. Zhang, S. Jia, A. Bansil, H. Lin, and M. Z. Hasan, Nat. Commun. **6**, 7373 (2015).

[2] T. Liang, Q. Gibson, M. N. Ali, M. H. Liu, R. J. Cava, and N. P. Ong, Nat. Mater. **14**, 280 (2015).

[3] M. Neupane, S.-Y. Xu, R. Sankar, N. Alidoust, G. Bian, C. Liu, I. Belopolski, T.-R. Chang, H.-T. Jeng, H. Lin, A. Bansil, F. Chou, and M. Z. Hasan, Nat. Commun. **5**, 3786 (2014).

[4] X. G. Wan, A. M. Turner, A. Vishwanath, and S. Y. Savrasov, Phys. Rev. B **83**, 205101 (2011).

[5] Z. Wang, H. Weng, Q. Wu, X. Dai, and Z. Fang, Phys. Rev. B **88**, 125427 (2013).

[6] Z. J. Wang, Y. Sun, X. Q. Chen, C. Franchini, G. Xu, H. M. Weng, X. Dai, and Z. Fang, Phys. Rev. B **85**, 195320 (2012).

[7] H. M. Weng, X. Dai, and Z. Fang, J. Phys.: Condes. Matter **28**, 303001 (2016).

[8] H. M. Weng, C. Fang, Z. Fang, B. A. Bernevig, and X. Dai, Phys. Rev. X **5**, 011029 (2015).

[9] S. Y. Xu, I. Belopolski, N. Alidoust, M. Neupane, G. Bian, C. L. Zhang, R. Sankar, G. Q. Chang, Z. J. Yuan, C. C. Lee, S. M. Huang, H. Zheng, J. Ma, D. S. Sanchez, B. K. Wang, A. Bansil, F. C. Chou, P. P. Shibayev, H. Lin, S. Jia, and M. Z. Hasan, Science **349**, 613 (2015).

[10] H. Zheng, S. Y. Xu, G. Bian, C. Guo, G. Q. Chang, D. S. Sanchez, I. Belopolski, C. C. Lee, S. M. Huang, X. Zhang, R. Sankar, N. Alidoust, T. R. Chang, F. Wu, T. Neupert, F. C. Chou, H. T. Jeng, N. Yao, A. Bansil, S. Jia, H. Lin, and M. Z. Hasan, ACS Nano **10**, 1378 (2016).

[11] T. R. Chang, S. Y. Xu, D. S. Sanchez, W. F. Tsai, S. M. Huang, G. Q. Chang, C. H. Hsu, G. Bian, I. Belopolski, Z. M. Yu, S. Y. A. Yang, T. Neupert, H. T. Jeng, H. Lin, and M. Z. Hasan, Phys. Rev. Lett. **119**, 026404 (2017).

[12] K. W. Chen, X. Lian, Y. Lai, N. Aryal, Y. C. Chiu, W. Lan, D. Graf, E. Manousakis, R. E. Baumbach, and L. Balicas, Phys. Rev. Lett. **120**, 206401 (2018).

[13] F. Fei, X. Bo, R. Wang, B. Wu, J. Jiang, D. Fu, M. Gao, H. Zheng, Y. Chen, X. Wang, H. Bu, F. Song, X. Wan, B. Wang, and G. Wang, Phys. Rev. B **96**, 041201(R) (2017).

[14] D. Fu, X. Bo, F. Fei, B. Wu, M. Gao, X. Wang, M. Naveed, S. A. Shah, H. Bu, B. Wang, L. Cao, W. Zou, X. Wan, and F. Song, Phys. Rev. B **97**, 245109 (2018).

[15] X. C. Pan, X. L. Chen, H. M. Liu, Y. Q. Feng, Z. X. Wei, Y. H. Zhou, Z. H. Chi, L. Pi, F. Yen, F. Q. Song, X. G. Wan, Z. R. Yang, B. G. Wang, G. H. Wang, and Y. H. Zhang, Nat. Commun. **6**, 7805 (2015).

[16] A. A. Soluyanov, D. Gresch, Z. J. Wang, Q. S. Wu, M. Troyer, X. Dai, and B. A. Bernevig, Nature (London) **527**, 495 (2015).

[17] S. Y. Xu, N. Alidoust, G. Q. Chang, H. Lu, B. Singh, I. Belopolski, D. S. Sanchez, X. Zhang, G. Bian, H. Zheng, M. A. Husanu, Y. Bian, S. M. Huang, C. H. Hsu, T. R. Chang, H. T. Jeng, A. Bansil, T. Neupert, V. N. Strocov, H. Lin, S. A. Jia, and M. Z. Hasan, Sci. Adv. **3**, e1603266 (2017).

[18] M. Z. Yan, H. Q. Huang, K. N. Zhang, E. Y. Wang, W. Yao, K. Deng, G. L. Wan, H. Y. Zhang, M. Arita, H. T. Yang, Z. Sun, H. Yao, Y. Wu, S. S. Fan, W. H. Duan, and S. Y. Zhou, Nat. Commun. **8**, 257 (2017).

[19] K. N. Zhang, M. Z. Yan, H. X. Zhang, H. Q. Huang, M. Arita, Z. Sun, W. H. Duan, Y. Wu, and S. Y. Zhou, Phys. Rev. B **96**, 125102 (2017).

[20] T. E. O'Brien, M. Diez, and C. W. J. Beenakker, Phys. Rev. Lett. **116**, 236401 (2016).

[21] M. N. Ali, J. Xiong, S. Flynn, J. Tao, Q. D. Gibson, L. M. Schoop, T. Liang, N. Haldolaarachchige, M. Hirschberger, N. P. Ong, and R. J. Cava, Nature (London) **514**, 205 (2014).

[22] M. Udagawa and E. J. Bergholtz, Phys. Rev. Lett. **117**, 086401 (2016).

[23] M. Hirschberger, S. Kushwaha, Z. J. Wang, Q. Gibson, S. H. Liang, C. A. Belvin, B. A. Bernevig, R. J. Cava, and N. P. Ong, Nat. Mater. **15**, 1161 (2016).

[24] Y. K. Luo, R. D. McDonald, P. F. S. Rosa, B. Scott, N. Wakeham, N. J. Ghimire, E. D. Bauer, J. D. Thompson, and F. Ronning, Sci. Rep **6**, 27294 (2016).

[25] J. Xiong, S. K. Kushwaha, T. Liang, J. W. Krizan, M. Hirschberger, W. D. Wang, R. J. Cava, and N. P. Ong, Science **350**, 413 (2015).

[26] F. Arnold, C. Shekhar, S.-C. Wu, Y. Sun, R. D. dos Reis, N. Kumar, M. Naumann, M. O. Ajeesh, M. Schmidt, A. G. Grushin, J. H. Bardarson, M. Baenitz, D. Sokolov, H. Borrmann, M. Nicklas, C. Felser, E. Hassinger, and B. Yan, Nat. Commun. **7**, 11615 (2016).

[27] R. D. dos Reis, M. O. Ajeesh, N. Kumar, F. Arnold, C. Shekhar, M. Naumann, M. Schmidt, M. Nicklas, and E. Hassinger, New J. Phys. **18**, 085006 (2016).

[28] A. A. Burkov, Phys. Rev. B **96**, 041110(R) (2017).

[29] S. Nandy, G. Sharma, A. Taraphder, and S. Tewari, Phys. Rev. Lett. **119**, 176804 (2017).

[30] N. Kumar, S. N. Guin, C. Felser, and C. Shekhar, Phys. Rev. B **98**, 041103(R) (2018).

[31] H. Li, H.-W. Wang, H. He, J. Wang, and S.-Q. Shen, Phys. Rev. B **97**, 201110(R) (2018).

[32] P. Li, C. H. Zhang, J. W. Zhang, Y. Wen, and X. X. Zhang, Phys. Rev. B **98**, 121108(R) (2018).

[33] D. Liang, Y. Wang, W. Zhen, J. Yang, S. Weng, X. Yan, Y. Han, W. Tong, L. Pi, W. Zhu, and C. Zhang, arXiv:1809.01290, 2018.

[34] R. Singha, S. Roy, A. Pariari, B. Satpati, and P. Mandal, Phys. Rev. B **98**, 081103(R) (2018).

[35] M. Wu, G. Zheng, W. Chu, Y. Liu, W. Gao, H. Zhang, J. Lu, Y. Han, J. Zhou, W. Ning, and M. Tian, Phys. Rev. B **98**, 161110(R) (2018).

[36] C. Xu, B. Li, W. Jiao, W. Zhou, B. Qian, R. Sankar, N. D. Zhigadlo, Y. Qi, D. Qian, F.-C. Chou, and X. Xu, Chem. Mater. **30**, 4823 (2018).

[37] See Supplemental Material at http://link.aps.org/supplemental/10.1103/PhysRevB.99.155119 for the calculated band structure and Fermi surface configurations.

[38] S. Liang, J. Lin, S. Kushwaha, J. Xing, N. Ni, R. J. Cava, and N. P. Ong, Phys. Rev. X **8**, 031002 (2018).

[39] A. A. Taskin, H. F. Legg, F. Yang, S. Sasaki, Y. Kanai, K. Matsumoto, A. Rosch, and Y. Ando, Nat. Commun. **8**, 1340 (2017).

[40] B. Wu, X.-C. Pan, W. Wu, F. Fei, B. Chen, Q. Liu, H. Bu, L. Cao, F. Song, and B. Wang, Appl. Phys. Lett. **113**, 011902 (2018).

[41] H. X. Tang, R. K. Kawakami, D. D. Awschalom, and M. L. Roukes, Phys. Rev. Lett. **90**, 107201 (2003).